Engineering Geology 235 (2018) 11–19

Contents lists available at ScienceDirect

Engineering Geology

journal homepage: www.elsevier.com/locate/enggeo

Assessment of the effects of historical strong earthquakes on large-scale landslide groupings in the Wei River midstream

T. Wang[a], S.R. Wu[a], J.S. Shi[a,b], P. Xin[a], L.Z. Wu[c,*]

[a] Institute of Geomechanics, Chinese Academy of Geological Sciences, Beijing 100081, China
[b] China Geological Survey, M.L.R., Beijing 100037, China
[c] State Key Laboratory of Geohazard Prevention and Geoenvironment Protection, Chengdu University of Technology, Chengdu, Sichuan 610059, China

ARTICLE INFO

Keywords:
Historical earthquake
Landslide
Loess
Wei River
Newmark displacement model

ABSTRACT

Regional active tectonics and historical earthquake records indicate the importance of the triggering effects of historical strong earthquakes on groups of large-scale landslide occurrences in the Wei River midstream section. In this study, a method to assess the triggering effects of historical earthquakes on regional large-scale landslides is presented. The greatest epicentral distances of seismically induced landslides were calculated. The triggering effects of four key historical strong earthquakes with epicenters within 300 km of the Wei River midstream section were analyzed; these are the M_s 7.0 Qishan earthquake of 780 BCE, the M_s 8.0 Tianshui earthquake of 1654 CE, the M_s 8.25 Huaxian earthquake of 1556 CE, and the M_s 8.5 Haiyuan earthquake of 1920 CE. Taking the Qishan earthquake as an example, a seismically induced landslide displacement and hazard assessment method based on the Newmark displacement model was developed. The degree of spatial matching of the results for historical-earthquake-triggered landslides and the distribution of actual large-scale landslide deposits were compared quantitatively using the success rate curve method. The results show that of the four historical earthquakes, the Tianshui earthquake had the strongest effect of inducing large-scale landslides regionally along the Wei River midstream section.

1. Introduction

The Loess Plateau in Northwest China was formed by the deposition of windblown dust. Loess is easily eroded, and many slope collapses, such as landslides, occur in areas with loess deposits (Ishihara et al., 1990; Jefferson et al., 2003; Wu et al., 2017; Zhang et al., 2017). The midstream section of the Wei River lies in the southern part of the Loess Plateau and at the western end of the Weihe seismic zone. Strong historical earthquakes have been reported in this area, and many of the landslides in the region were triggered by such earthquakes (Derbyshire, 1991; Zhang et al., 2017). Seismically induced landslides make up a relatively high proportion (> 50%) of all loess landslides in Northwest China. Study of the effects of historical strong earthquakes on clusters of large landslides is of great significance to earthquake disaster mitigation.

Major earthquakes, such as the 1994 Northridge earthquake in the USA (Harp and Jibson, 1996), the 1999 Chi-Chi earthquake in Taiwan (Lee et al., 2008), the 2005 M_w 7.6 Kashmir earthquake in Pakistan (Sato et al., 2007; Owen et al., 2008), the 2008 M_w 7.9 Wenchuan earthquake in China (Huang and Li, 2009; Xu et al., 2014), the 2010 M_w 7.0 Port-au-Prince earthquake in Haiti (Gorum et al., 2014), and the 2011 M_w 9.0 Tohoku-Oki earthquake in Japan (Wartman et al., 2013), have induced a large number of high-intensity, large-scale landslides, which have caused great loss of life and property. In recent years, earthquake-triggered landslides have received increasing attention in the fields of active tectonics, geomorphology, engineering geology, and environmental geology (Keefer, 1984, 2002; Rodríguez et al., 1999; Harp et al., 2011; Guzzetti et al., 2012; Xu et al., 2012, 2014; Lee et al., 2008; Grant et al., 2016; Saade et al., 2016). Several studies have been conducted on groups of loess landslides; these studies have focused mainly on the structure, formation conditions, and evolution of such landslides (Derbyshire, 1991; Dijkstra et al., 1994; Shi et al., 2016). However, the triggering factors of landslides linked to historical strong earthquakes have rarely been examined. The specific strong-earthquake processes that induced these landslides have not been evaluated previously. In fact, analyses of historical earthquakes are often based on studies of earthquake-induced landslides; therefore, it is important to investigate the landslide-inducing processes generated by historical strong earthquakes to understand the formation mechanisms of groups of earthquake-induced landslides.

The effects of the 2008 M_w 7.9 Wenchuan earthquake on the midstream section of the Wei River provide new opportunities to

* Corresponding author.
E-mail addresses: wangtaoig@cags.ac.cn (T. Wang), shrwu@cags.ac.cn (S.R. Wu), sjusong@mail.cgs.gov.cn (J.S. Shi), wulizhou07@cdut.cn (L.Z. Wu).

https://doi.org/10.1016/j.enggeo.2018.01.020
Received 23 May 2017; Received in revised form 18 January 2018; Accepted 21 January 2018

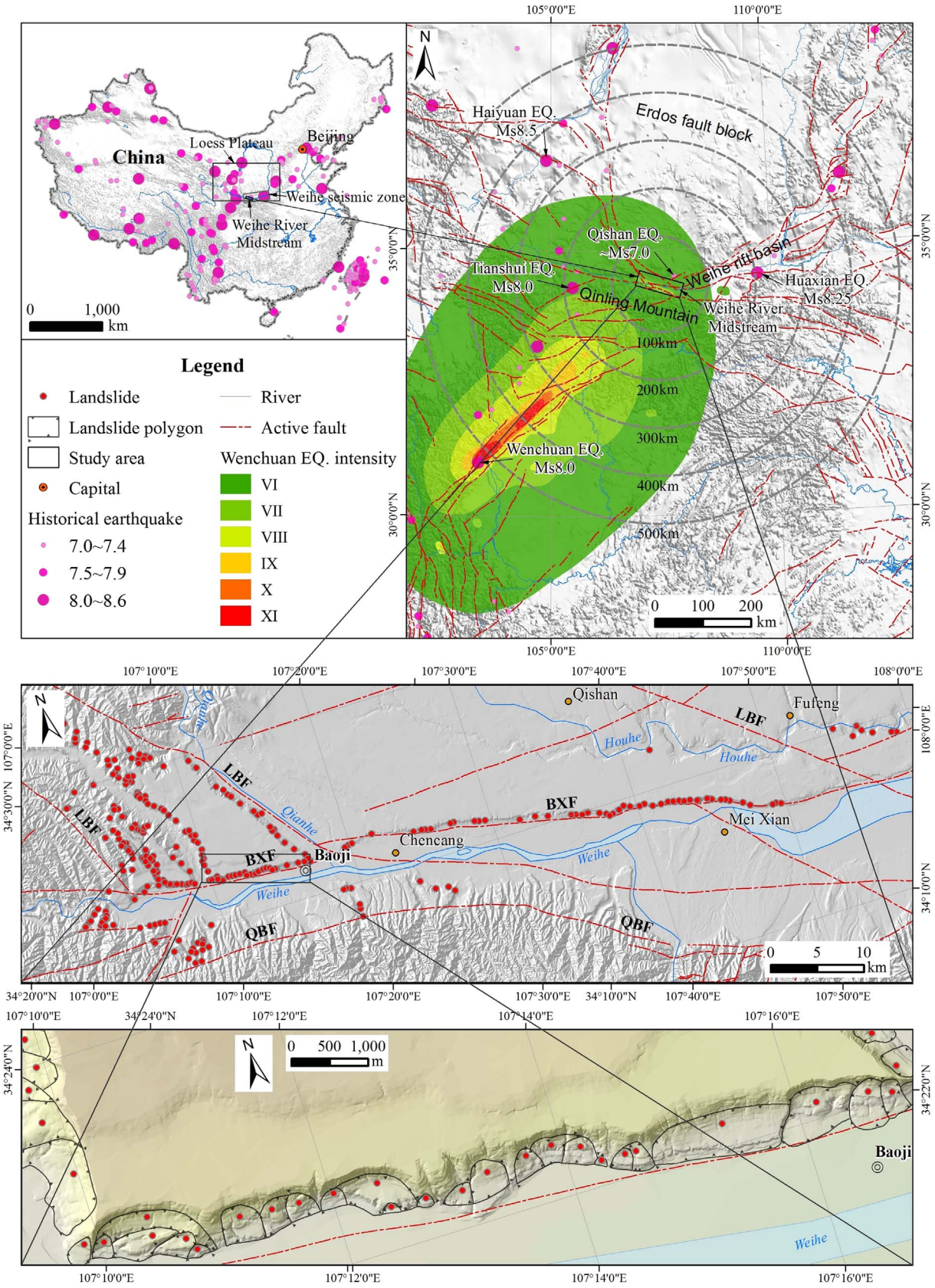

Fig. 1. Distribution of active faults and historical epicenters around the midstream section of the Wei River. QBF: North Qinling rim fault zone; BXF: Baoji–Xianyang fault zone; WBF: North Weihe Basin rim fault zone; LBF: Longxian–Baoji fault zone.

understand earthquake-induced landslides. Although the Wei River midstream section is about 520 km from the epicenter of the Wenchuan earthquake and separated from it by the Qinling fold system, abnormally strong ground motion of intensity VII appeared in this area, accompanied by intensity-VI movement in the outlying area (Fig. 1). A series of secondary geological events, including landslides, collapses, and sand liquefaction, were triggered in the Wei River midstream section by the Wenchuan earthquake. At least four historical strong earthquakes of M 8.0–8.5 were recorded in the region within about 500 km of the Wei River midstream section. The epicenters of all of these events were located in the same tectonic location as the Weihe Basin or adjacent to it (Fig. 1). By analyzing the Wenchuan earthquake in terms of magnitude, epicentral distance, and tectonic setting, we can infer the ground motions of historical strong earthquakes that occurred in the surrounding area that could induce large numbers of ancient landslides in the Wei River midstream section.

In this paper, we present qualitative and quantitative methods to examine the triggering factors of historical strong earthquakes that induced loess landslides, based on earthquake magnitude and epicenter data. The relationship between groups of loess landslides and historical strong earthquakes in the Wei River midstream section is discussed, and the factors associated with historical strong earthquakes that triggered loess landslides are analyzed.

2. Materials and methods

2.1. Active tectonic setting

The midstream section of the Wei River is located at the southern edge of the Loess Plateau, in the vicinity of the Weihe and Liupanshan seismic zones, which corresponds to the eastern part of the North–South Seismic Zone. Several historical strong earthquakes have occurred in this area (Fig. 1), and resulted in numerous catastrophic landslides where loose structures and weak loess slopes were affected by seismic loading. These landslides include the Dangjiacha landslide caused by the 1920 Haiyuan earthquake in Ningxia Province (Fig. 1), the Luojiabu landslide that resulted from the 1654 Tianshui earthquake in Gansu Province (Fig. 1), and the Yongning landslide associated with the 1718 Tongwei earthquake in Gansu Province.

The central part of the Wei River midstream section is located in the Weihe Basin. There are three active fault zones in the region, spread from south to north: the Qinling northern margin fault zone, the Baoji–Xianyang fault zone, and the Longxian–Baoji fault zone (Fig. 1). The Weihe rift basin has been the locus of regional tectonic activity over approximately the last 3000 years, and was the source of most of the earthquakes in the region and all of the strong earthquakes in Shaanxi Province. In areas of loess-covered slopes along the midstream section of the Wei River, the structural control of active faults on landslides is also crucial. For example, during the Wenchuan earthquake, a straight, 500-m-long ground fracture formed along the Qianhe Fault in the Longxian–Baoji fault zone on the western side of the Qian River. On the edge of the Loess Plateau, on the left side of the Wei River midstream section, surficial secondary faults of the Baoji–Xianyang fault zone cut through shallow loess and paleosol layers (Shi et al., 2016). This faulting resulted in a fractured structure and weakened the soil mass. Because the fragmented loess mass in the fault zone is prone to deformation, large-scale landslides are very likely to occur during an earthquake in this area. Regional active tectonics control the earthquake characteristics, and local active faults control the landslide type. Understanding the effects of historical strong earthquakes that have induced clusters of large-scale landslides in the Wei River midstream section can provide insight into landslide triggering risks.

2.2. Landslide mapping

A digital elevation model (DEM) with 5-m resolution and QuickBird satellite imagery with 0.61-m resolution, combined with field survey data, were used to map loess landslide deposits in the Wei River midstream section (Fig. 1). Most of these landslide deposits lie on the banks of the Wei River and its tributaries in the western region of the study area. The landslide deposits were mapped as polygons (Fig. 1, lower panel) with a single point representing each landslide on a regional scale in the spatial analysis model.

Most of these large-scale landslides formed nearly vertical scarps and horizontal depositional characteristics. Because most of these landslide events were ancient or old, the original slope gradients (before sliding) were unavailable. Consequently, it is difficult to evaluate the landslide formation mechanisms. Therefore, we generally positioned the landslide point at the transition zone between the landslide scarp and the deposit area. Thus, we estimate that the landslide point represents the average gradient of the original slope.

It should be noted that the mapped landslides in the Wei River midstream section were identified based on remote sensing techniques and field surveying. The basic morphology and structural characteristics of the loess landslides could still be recognized after multiple land movements and landform changes. However, traces of the landslides induced by prehistoric earthquakes are typically poorly preserved and can be difficult to distinguish; therefore, these cases have not been considered here.

3. Epicentral distances of major historical strong earthquakes

In western China, large-scale catastrophic seismic landslides have occurred mainly in the meizoseismal areas of earthquakes of $> M_s$ 7.0. To analyze the effects of earthquakes that induce large landslides in this region, we have examined relevant earthquakes with various magnitudes associated with large landslides, especially earthquakes with magnitudes above M_s 7.0. Based on an empirical relationship between earthquake magnitude and the epicentral distances of the triggered landslides, we can identify historical strong earthquakes that were strongly related to landslides in the region.

Wang et al. (1999) analyzed 81 earthquakes of M_s 5.5–8.5 that induced loess landslides in Shaanxi, Gansu, Ningxia, and Shanxi provinces. The results show that the epicentral distances of densely spaced large landslides (100–1000 $\times$ 10^4 m^3) may exceed 140 km for M_s 8.5 earthquakes, whereas smaller landslides ($< 10 \times 10^4$ m^3) may have epicentral distances of over 300 km. The maximum epicentral distance (D_e) of a landslide is expressed as:

$$\log D_e = 12.82 \log M_w - 9.508 \quad \text{(for areas of high landslide density)} \tag{1a}$$

$$\log D_e = 9.90 \log M_w - 6.332 \quad \text{(for areas of low landslide density)} \tag{1b}$$

These empirical equations of seismic landslide distributions were derived based on densely spaced large landslides and sparsely distributed small landslides, respectively (Wang et al., 1999) (Table 1). A total of 194 landslides induced by 71 historical earthquakes across all of western China were analyzed by Sun et al. (2004) to determine maximum epicentral distance:

Table 1
Greatest epicentral distances of loess landslides induced by earthquakes of various magnitudes.

Earthquake magnitude (M_s)	Greatest epicentral distance (km)			
	D_e (area of landslide concentration)	D_e (area of landslide dispersion)	D_e	
7.0	21	108	211	236
7.5	51	215	278	305
8.0	117	263	358	375
8.5	140	310	455	445

$$D_e = 3000\left[1 - \frac{4}{M_S}\right]^3 \quad (M_S \geq 4) \tag{2a}$$

Based on the same historical earthquake and seismic landslide data, an empirical equation for the maximum epicentral distance D_e of a seismic landslide caused by an earthquake of $7.0 \leq M_s \leq 8.6$ was proposed by Sun et al. (2004):

$$D_e = 9.816 \times 10^{-2} M_S^{3.9442} \quad (7.0 \leq M_S \leq 8.6) \tag{2b}$$

Eq. (1) provides good estimates of the maximum epicentral distances of seismic landslides for loess landslides in the Wei River region. The midstream section of the Wei River is a typical loess area; therefore, the correlation coefficient between the landslides and epicentral distances is high at 0.91. To ensure that all major historical earthquakes in the region were accounted for, we considered the situation of maximum epicentral distances for sparsely distributed seismic landslides. We examined the records of historical strong earthquakes and selected earthquakes based on the optimal combination of magnitude and epicentral distance from the Wei River midstream section. The 1920 Haiyuan earthquake (M_s 8.5) was chosen within the 300-km range, with the 1654 Tianshui (M_s 8.0) and the 1556 Huaxian (M_s 8.25) earthquakes within 250 km, and the Qishan earthquake (M_s 7.0) within 100 km of the study region. The relevant seismic parameters are shown in Fig. 1 and Table 2. These data were used for quantitative assessment of the effects of historical strong earthquakes that induced landslides in the region. Because large-scale catastrophic seismic landslides have mainly occurred in the meizoseismal areas of earthquakes above M_s 7.0, landslides induced by historical earthquakes below M_s 7.0 were not considered. Table 2 lists the focal depths of the Tianshui, Huaxian, and Haiyuan earthquakes. The focal depth of the Qishan earthquake was determined based on the following factors: (1) the average focal depth in the North China seismotectonic region where the Qishan earthquake occurred is 14 ± 7 km; (2) the seismogenic structure of the Qishan earthquake is located on the southwest edge of the Erdos block, where the focal depth is generally deeper than the average depth; (3) we referred to the focal depth data of modern earthquakes neighboring the Qishan earthquake. Based on these factors, the focal depth of the Qishan earthquake was estimated as 17 km.

4. Assessment of the effects of historical earthquakes on landslides

To quantitatively evaluate the effects of the four historical strong earthquakes that induced landslides in the Wei River midstream section, the Newmark displacement model (Wieczorek et al., 1985; Jibson, 1993; Jibson et al., 2000; Roberto, 2000; Refice and Capolongo, 2002; Godt et al., 2008; Grant et al., 2016) was used to assess seismic landslide hazards. This assessment consisted of the following steps (Fig. 2). a) The factor of safety (F_s) for slopes in the region was calculated according to the soil strength and slope geometry. b) The critical acceleration (a_c) of the slope under the limit equilibrium condition was calculated, assuming seismic loading with F_s and the terrain slope. c) The regional ground motion Arias intensity (I_a) distribution during the earthquake was computed and combined with moment magnitude (M_w) and hypocentral distance (R) data. d) The accumulated sliding displacement on the regional slopes due to seismic loading, which can be approximated using regression equations (Hsieh and Lee, 2011; Du and Wang, 2016; Song et al., 2017), was analyzed to assess seismic landslide hazards. The Qishan earthquake was taken as an example to assess the seismic landslide hazard.

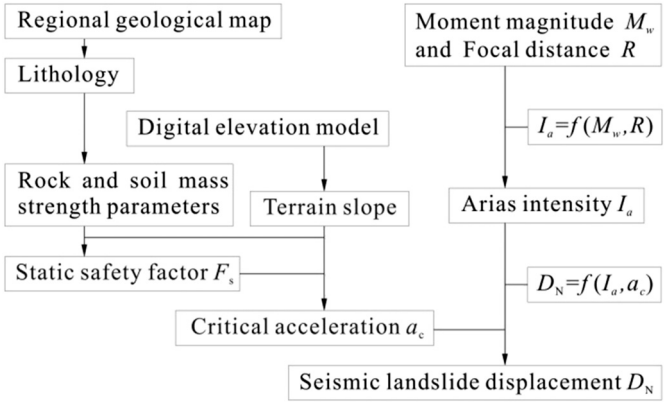

Fig. 2. Risk assessment flowchart for seismic landslides based on the simplified Newmark displacement model.

4.1. The static factor of safety

Newmark's sliding rigid-block model simplifies slope instability as a rigid block sliding on a planar surface. The capacity of the slope to resist seismic shaking can be expressed by the static factor of safety. We used a relatively simple limit-equilibrium model of an infinite slope (Prior and Suhayda, 1979; Grant et al., 2016; Saade et al., 2016). The assumptions involved in this model are the following: (1) the sliding mass is assumed to be a rigid plastic body; (2) the static factor of safety is not strain-dependent and thus remains constant throughout the analysis; (3) the static and dynamic shear resistances are considered to be the same and constant; (4) the effects of dynamic pore pressure are negligible, (5) the soil properties are homogeneous.

According to the limit equilibrium theory, the static factor of safety F_s can be obtained as follows (Jibson et al., 2000):

$$F_s = \frac{c'}{\gamma t \sin\alpha} + \frac{\tan\varphi'}{\tan\alpha} - \frac{m\gamma_w \tan\varphi'}{\gamma \tan\alpha}, \tag{3}$$

where c' is the effective cohesion [MPa]; γ is the unit weight of the rock and soil mass [N/m^3]; t is the thickness of the potential sliding mass [m]; α is the dip angle of the potential sliding surface [°]; φ' is the effective internal friction angle [°]; m is the saturation proportion of the whole potential sliding mass thickness; and γ_w is the unit weight of the groundwater [N/m^3].

The regional geological map (1:250,000) of the Wei River midstream region was vectorized (Fig. 3). Based on comparison of landslide distribution (Fig. 1) and regional lithology data, most of the landslides occurred in Quaternary loess and Neogene mudstone strata. The physico-mechanical parameters of the soil were obtained by sampling undisturbed cores and performing laboratory tests (Tan et al., 2015). The empirical physico-mechanical parameters of other rock and soil masses were obtained from the literature (Table 3) (Tan et al., 2015). Based on

Table 2
Basic characteristics of key historical strong earthquakes around the Wei River midstream section.

No.	Location of epicenter	Coordinates	Earthquake magnitude (M_s)	Focal depth (km)	Epicentral distance (km)	Direction
1	Qishan, Shanxi	34.5°N, 107.8°E	7.0	~17	35	NEE
2	Tianshui, Gansu	34.3°N, 105.5°E	8.0	20	181	WSW
3	Huaxian, Shanxi	34.5°N, 109.7°E	8.25	25	206	ENE
4	Haiyuan, Ningxia	36.5°N, 105.7°E	8.5	17	288	NW

The epicentral distance is from the central region of the Wei River to the epicenter; and the direction is toward the epicenter from the center of the study area.

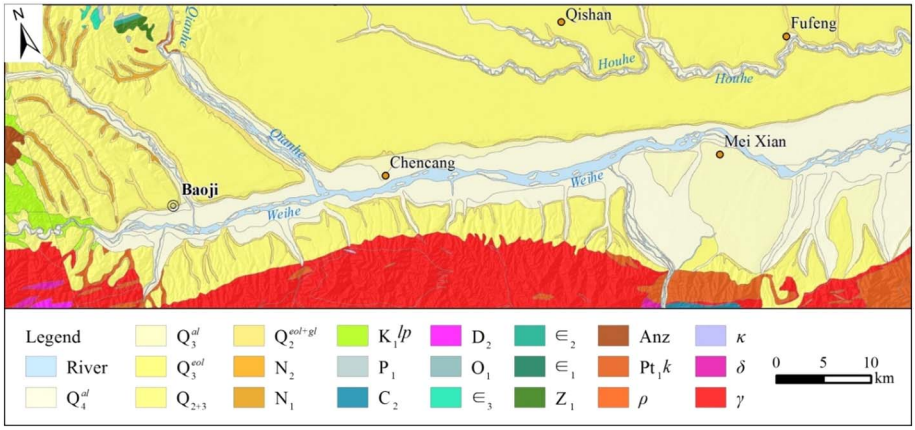

Fig. 3. Formation lithologies in the vicinity of the Wei River midstream section. Q_4^{al}: Quaternary Holocene alluvial plain; Q_3^{al}: Quaternary Upper Pleistocene Taibai Formation; Q_3^{eol}: Quaternary Upper Pleistocene Malan Formation; Q_{2+3}: Quaternary Middle-Upper Pleistocene; Q_2^{eol+gl}: Quaternary Middle Pleistocene; N_2: Neogene Pliocene; N_1: Neogene Miocene; K_1lp: Lower Cretaceous Liupanshan Group; P_1: Lower Permian; C_2: Middle Carboniferous; D_2: Middle Devonian; O_1: Lower Ordovician; $\in_3$: Upper Cambrian; $\in_2$: Middle Cambrian; $\in_1$: Lower Cambrian; Z_1: Lower Sinian; AnZ: pre-Sinian, Pt_1k: Lower Proterozoic Kuanping Group; ρ: pegmatite vein; *k*: lamprophyre vein; *δ*: quartz diorite; γ: granite.

Table 3
Geotechnical parameters of lithologies in the Wei River midstream region.

No.	Symbol	γ (kN/m^3)	c′ (MPa)	φ′ (°)
1	Q_4^{al}	20.5	0.03	13.0
2	Q_3^{al}	18.3	0.04	26.0
3	Q_3^{eol}	17.3	0.04	24.0
4	Q_{2+3}	18.4	0.05	27.3
5	Q_2^{eol+gl}	18.5	0.07	28.5
6	N_2	23.0	0.18	30
7	N_1	23.5	0.20	33
8	K_1lp	25.5	1.1	45
9	P_1	26.0	1.3	48
10	C_2	26.5	1.5	50
11	D_2	27.5	2.0	60
12	O_1	26.5	1.8	55
13	$\in_3$	26.0	1.6	53
14	$\in_2$, $\in_1$	24.0	0.6	35
15	Z_1	26.5	1.5	50
16	*Anz*	27.5	2.0	60
17	Pt_1k	26.8	2.0	59.5
18	γ, ρ, κ, *δ*	27.5	2.1	60

Eq. (3) and a raster overlay calculation using a geographic information system (GIS), we obtained the F_s distribution of the slopes in the region of the Wei River midstream section (Fig. 4). The results show that F_s values for relatively flat areas exceed 10 (the green area in Fig. 4) with adequate slope stability. In the central-southern and western sections with steep slopes, F_s values are low, < 1.0 in certain areas (the red area in Fig. 4), which indicate slopes prone to failure.

4.2. Critical slope acceleration

The ground motion acceleration in the limit equilibrium condition of a potential sliding block is denoted as the critical acceleration a_c. By comparing the block stress states under a static force and seismic load, and constructing a force analysis equation for the sliding block under seismic loading, a_c can be defined as a function of the static safety factor F_s (Wilson and Keefer, 1983):

$$a_c = (F_s - 1)g \sin a, \quad (4)$$

where g is the acceleration due to gravity [m/s^2] and a is the dip angle of the sliding surface [°], which is approximately equal to the slope angle. In this case, a_c shows the slope sliding potential due to slope properties that are inherent under an assumed seismic load. Therefore, it can be used as the basis for regional seismic landslide susceptibility assessment.

4.3. Ground motion Arias intensity

The topographic amplification of ground motion results in an irregular distribution of seismically induced landslides (Hartzell et al., 1994; Sepúlveda et al., 2005; Murphy, 2006; Huang and Li, 2009). For the Qishan earthquake, we calculated the ground motion Arias intensity and its topographic amplification, and thus obtained the distribution of synthetic ground motion Arias intensity. The Arias intensities of the other three historical earthquakes were also calculated, with topographic amplification effects taken into consideration.

4.3.1. Topographic amplification of ground motion

The topographic amplification effect for a locally prominent terrain can be described as (The Ministry of Construction of the People's Republic of China, 2002):

$$\lambda = 1 + \xi \times \alpha, \quad (5)$$

where λ is the amplification coefficient of the seismic influence coefficient at the top of a localized prominent terrain, α is the increase in amplitude of the ground motion in the local terrain, and ξ is an additional adjustment coefficient. The parameter α can be approximated from the slope height and slope gradient (Table 4), and ξ is set to 1.0 for simplicity. We calculated the slope height and slope gradient distribution using a regional DEM (5-m resolution), and then calculated the

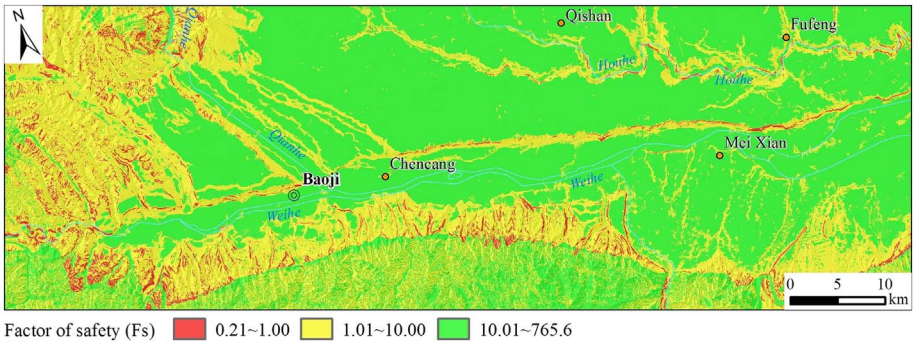

Fig. 4. Factors of safety F_s of slopes in the vicinity of the Wei River midstream section. (For interpretation of the references to color in this figure, the reader is referred to the web version of this article.)

Table 4
The empirical amplification coefficients of ground motion for slopes.

H (m)	Soil slope	$H < 5$	$5 \le H < 15$	$15 \le H < 25$	$H \ge 25$
	Rock slope	$H < 20$	$20 \le H < 40$	$40 \le H < 60$	$H \ge 60$
H/L	$H/L < 0.3$	0	0.1	0.2	0.3
	$0.3 \le H/L < 0.6$	0.1	0.2	0.3	0.4
	$0.6 \le H/L < 1.0$	0.2	0.3	0.4	0.5
	$H/L \ge 1.0$	0.3	0.4	0.5	0.6

Note that H is the slope height and H/L is the tangent of the slope.

amplification coefficient for the ground motion at a locally prominent terrain in the Loess Plateau and in a hilly area of the Wei River midstream section using Eq. (5).

4.3.2. Synthetic ground motion Arias intensity

The Arias intensity (I_a) is expressed as (Arias, 1970; Harp and Wilson, 1995):

$$I_a = \frac{\pi}{2g}\int_0^{T_d} [a(t)]^2 dt, \tag{6}$$

where $a(t)$ is the ground motion acceleration in an arbitrary directional component of the strong-motion record associated with the four earthquakes [m/s^2], and T_d is the total duration of the ground motion acceleration record [s].

Thus, I_a includes the ground motion amplitude, frequency, and duration. It shows a positive correlation with ground motion energy attenuation (Arias, 1970). However, the commonly used peak ground acceleration (PGA) parameter only indicates amplitudes with high frequencies and short durations in the ground-motion record, and ignores the frequency intervals and durations of ground-motion-inducing landslides. Therefore, I_a is more favorable than PGA for analyzing the correlation between regional seismic landslides and ground motion intensity. It is difficult to obtain accurate ground motion data for historical earthquakes, but I_a can be calculated using the following empirical equation (Wilson and Keefer, 1985; Keefer and Wilson, 1989):

$$\log I_a = \begin{cases} M_w - 2\log R - 4.1 & M_w \le 7.0 \\ 0.75M_w - 2\log R - 2.35 & M_w > 7.0 \end{cases}, \tag{7}$$

where M_w is the moment magnitude and R is the site hypocentral distance.

The value of M_w is related to the surface-wave magnitude M_s (Jin and Huang, 1996):

$$M_w = 0.844M_S + 0.951. \tag{8}$$

Eq. (8) was used to calculate the moment magnitude of the Qishan earthquake as $M_w = 6.86$. The corresponding Arias intensity in the midstream section of the Wei River caused by the Qishan earthquake can be determined using Eq. (8). By superimposing the amplification coefficient of ground motion on the terrain, the synthetic Arias intensity distribution in the region of the Qishan earthquake was obtained.

4.4. Landslide displacement under seismic loading

The displacement of regional seismically induced landslides based on the Newmark model can be calculated using a_c and I_a (Jibson, 1993; Jibson et al., 2000), and the landslide displacement (D_N) can be expressed as

$$\log D_N = 1.521 \log I_a - 1.993 \log a_c - 1.546 \tag{9}$$

Based on calculation of seismic landslide displacement and Eq. (9), a regional landslide displacement ($\log D_N$) distribution associated with the M_s 7.0 Qishan earthquake was obtained for the midstream section of the Wei River (Fig. 5). The landslide displacement index is classified based on an empirical threshold of slope failure. For example, the landslide displacement index of 0.61 corresponds to displacement of about 4 cm, which is prone to slope failure. It is clear that landslide occurrences were concentrated mainly in the large displacement area. The locations of large seismic landslide displacement or high-hazard zones mainly lie along the edge of the Loess Plateau, loess-covered hilly areas, and steep southern slopes in the piedmonts of the Qinling Mountains. The moderate-hazard zones are located mainly in the central-eastern flat loess tableland and the wide, gently sloping Wei River valley area. The low-hazard zones are concentrated in the southwestern Qinling region, the Longshan Mountain bedrock area, and the local loess-covered tableland.

5. Comparison of the induced landslide effects of major historical earthquakes

Although landslide displacement and distribution of damage zones resulting from the M_s 7.0 Qishan earthquake can be assessed, the triggering effects of the earthquake on landslide occurrences still cannot be evaluated quantitatively. We classified the seismically induced landslide displacements into 25 grades (numbered 1 to 25) using equally sized quantile intervals, calculated the area of each displacement grade, counted the corresponding landslides in each area, and thus calculated the landslide density for each displacement grade. Fig. 6A depicts the correlation between landslide density and displacement for the Qishan earthquake. The results indicate that landslide density gradually decreased as landslide displacement decreased.

The distributions of landslide displacement in the midstream section of the Wei River caused by the four historical earthquakes included in this study were calculated using back analysis. The results for seismic landslide displacement were then compared with surveyed landslide density data (Fig. 6B–D). The shapes of the statistical histograms transition gradually from a bimodal wave pattern to unimodal decrease.

To quantitatively describe the diversity of the earthquake effects, the results (Fig. 7) for hazards associated with the four seismically induced landslides were correlated with the surveyed landslide deposits using the success rate curve (SRC) method. The SRC method is generally used to examine the efficiency of landslide hazard assessment (Chung and Fabbri, 1999; Conoscenti et al., 2008; Kamp et al., 2008; Corominas et al., 2014). Based on the success rate, the degree of spatial matching between the assessment and actual landslide occurrences induced by historical earthquakes can be quantitatively evaluated. The value interval of the SRC is 0% to 100%. Larger SRC values indicate better matching. The shape of the SRC shows that the degree of matching can be clearly divided into two categories. SRC values for the Haiyuan and Tianshui earthquakes are 0.80 and 0.81, respectively, and those of the Qishan and Huaxian earthquakes are only 0.60 and 0.72, respectively. The results for seismic landslide hazards associated with the Haiyuan and Tianshui earthquakes indicate better matches than those for the Qishan and Huaxian earthquakes. The degree of matching reflects the extent to which the surveyed landslides were induced by seismic events — better matching represents stronger seismically induced effects. Based on this analysis, the inducing effects of the four historical strong earthquakes linked to large landslide deposits in the midstream section of the Wei River can be listed from strongest to weakest in this order: the Tianshui, Haiyuan, Huaxian, and Qishan earthquakes.

The success rate curves described above were constructed from all areas, including slope and flat land. For more rigorous consideration, we developed additional success rate curves with the flat area with slopes $\le 5^\circ$ removed (Fig. 8). Comparison between Figs. 7 and 8 shows that three success rate values decreased and one success rate value increased. Despite changes in success rates in Fig. 8, the overall order of the success rates remained the same as that in Fig. 7. Thus, through two different analyses of success rate curves, it was further confirmed the landslide-inducing effects of the four historical earthquakes linked to

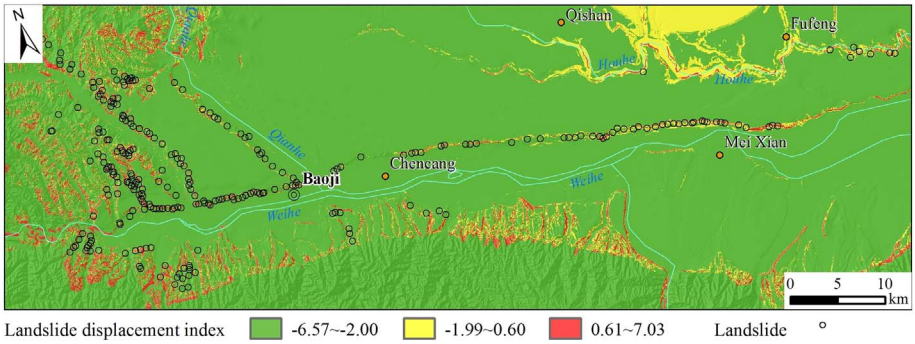

Fig. 5. Displacement and risk of landslides induced by the Qishan earthquake in the vicinity of the Wei River midstream section.

previous landslide occurrences in study area can be listed from strongest to weakest in the same order as above.

Not all of the large landslides identified in the study region can be linked to seismic events. Even though strong historical earthquakes have affected the entire midstream section of the Wei River, it is still very difficult to link each particular landslide to a specific historical earthquake using available techniques. The effects of historical earthquakes on large landslide occurrences in the region cannot be neglected, but specific results are often difficult to obtain from analyses of individual landslides. However, the statistical characteristics of regional landslide distributions can essentially distinguish between strong and weak triggering effects of strong historical earthquakes on large landslide occurrences using empirical and quantitative methods.

Our analysis of historical earthquakes that have induced landslides in this region shows that landslide mechanisms triggered by earthquakes are generally controlled by several factors, including magnitude, energy-spreading distance, site conditions, and occurrence time. Of the four strong historical earthquakes in this region, the most intense in terms of landslide induction was the M_s 8.0 Tianshui earthquake, rather than the M_s 8.5 Haiyuan earthquake, which had the strongest

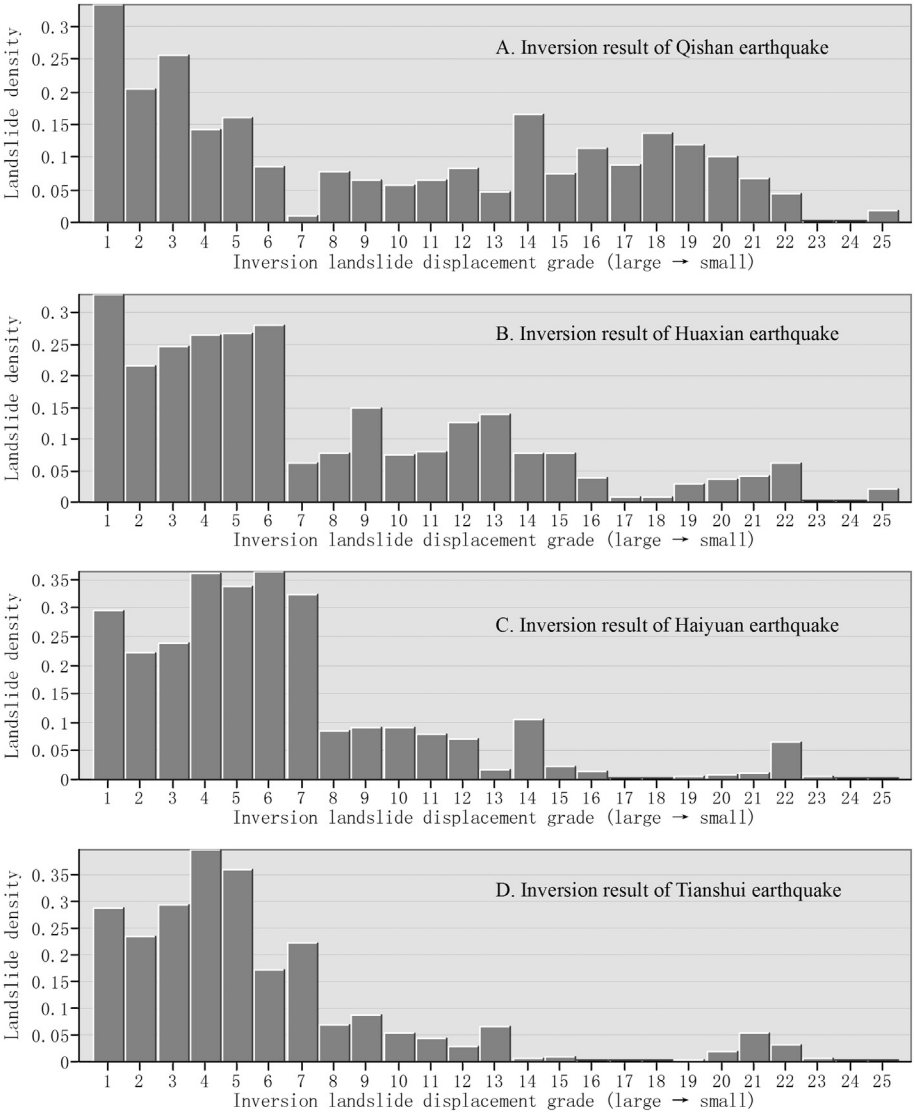

Fig. 6. Correlation between real landslide density and inverted historical earthquake landslide displacements. A. Qishan earthquake; B. Huaxian earthquake; C. Haiyuan earthquake; D. Tianshui earthquake.

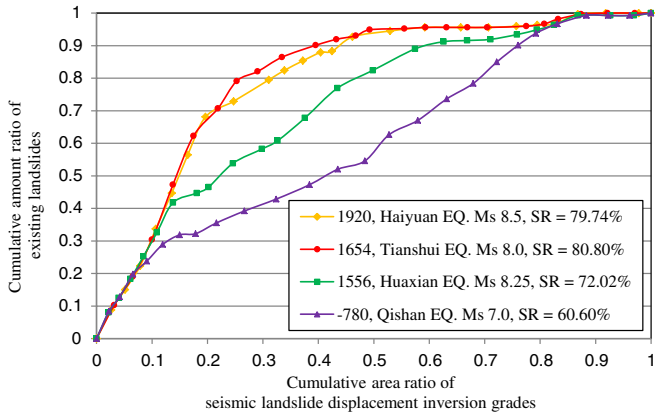

Fig. 7. Success rate curves showing the triggering effects of major historical strong earthquakes on large-scale landslide occurrences in the vicinity of the Wei River midstream section (including flat area).

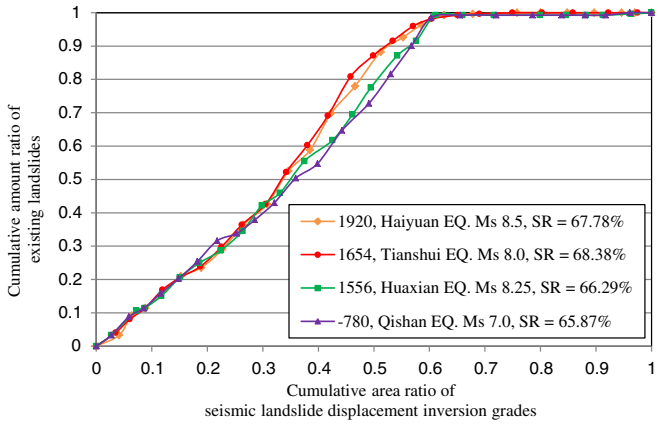

Fig. 8. Success rate curves showing the triggering effects of major historical strong earthquakes on large-scale landslides in the vicinity of the Wei River midstream section (flat area with slope ≤ 5° excluded).

magnitude and occurred most recently, or the M_s 7.0 Qishan earthquake, which was located closest to the study area.

6. Discussion

We have developed a new approach to explore the relation between historical earthquakes and regional landslide occurrences. The link between landslides and induction of historical earthquakes was examined; crucial induction effects of landslides caused by four historical earthquakes were screened, and seismically induced regional landslide displacements were assessed using the Newmark model. Despite the above achievements, some issues require further discussion.

We employed the empirical Arias intensity attenuation equation developed by Wilson and Keefer (Wilson and Keefer, 1985; Keefer and Wilson, 1989). One reason this equation was used is that there is limited knowledge about the spatial variability and attenuation characteristics of Arias intensity because of the lack of a strong ground motion record in China. The other reason is that most recently proposed attenuation equations require site factors such as the Vs30 value, which are difficult to acquire because of insufficient borehole data in this study area.

For the empirical estimation of Newmark displacement models, the Jibson model is widely used. Dreyfus et al. (2003) compared seven different empirical Newmark displacement models with an inventory of observed landslides from the 1994 Northridge, California earthquake (Dreyfus et al., 2003). Their results show that the accuracy of the predictive models depends primarily on the uncertainty of the model parameters, particularly shear strength.

Based on the above analysis and the geological background of the Wei River midstream area, these large-scale landslides are inferred to be highly correlated with earthquake events. Unfortunately, few records of these earthquakes exist, and no seismic landslide catalog is available. Therefore, it is difficult to examine which earthquakes caused which landslides. Because of this challenge, the cumulative effects of repeated earthquakes on the stability of the loess slopes are also quite difficult to evaluate. In the future, breakthroughs may be made by recording case studies of typical seismic landslides.

7. Conclusions

(1) Through application of analytical methods to the spatial distribution of the greatest epicentral distances of landslides affected by strong earthquakes in the midstream section of the Wei River, four major historical earthquakes that induced such landslides in the region were examined. Based on the Newmark displacement model and analysis of topographic ground-motion amplification effects, regional landslide displacements and hazard distributions for the four historical earthquakes were assessed.

(2) The correlation between historical seismic landslides and the distribution of existing large landslides were compared using the success rate curve method. The correlation results show that the triggering effects of the four historical strong earthquakes on large landslide occurrences in the midstream section of the Wei River can be arranged in order from strongest to weakest as: the Tianshui, Haiyuan, Huaxian, and Qishan earthquakes.

Acknowledgements

This study was funded by the National Natural Science Fund [grant numbers 41572313 and 41102165], the National 12th Five-Year Science and Technology Support Program [grant numbers 2012BAK10B02 and 2011BAK12B09], and the Land Resources Survey Project [grant number 12120114035501]; the corresponding author would like to thank the Innovation Team of Chengdu University of Technology.

References

Arias, A., 1970. A measure of earthquake intensity. In: Seismic Design for Nuclear Power Plants. Massachussetts Institute of Technology Press, Cambridge, MA, pp. 438–483.
Chung, C.F., Fabbri, A.G., 1999. Probabilistic prediction models for landslide hazard mapping. Photogramm. Eng. Remote. Sens. 65 (12), 1389–1399.
Conoscenti, C., Maggio, C.D., Rotigliano, E., 2008. GIS analysis to assess landslide susceptibility in a fluvial basin of NW Sicily (Italy). Geomorphology 94, 325–339.
Corominas, J., Westen, C., Frattini, P., Cascini, L., Malet, J.P., Fotopoulou, S., Catani, F., Eeckhaut, M., Mavrouli, O., Agliardi, F., Pitilakis, K., Winter, M.G., Pastor, M., Ferlisi, S., Tofani, V., Hervás, J., Smith, J.T., 2014. Recommendations for the quantitative analysis of landslide risk. Bull. Eng. Geol. Environ. 73 (2), 209–263.
Derbyshire, E., 1991. Landslides in the Gansu loess of China, loess-geomorphological hazards and processes. Catena Suppl. 20, 119–145.
Dijkstra, T.A., Rogers, C.D.F., Smalley, I.J., Derbyshire, E., Li, Y.J., Meng, X.M., 1994. The loess of north-central China: geotechnical properties and their relation to slope stability. Eng. Geol. 36, 153–171.
Dreyfus, D., Rathje, E.M., Jibson, R.W., 2003. The influence of different simplified sliding-block models and input parameters on regional predictions of seismic landslides triggered by the Northridge earthquake. Eng. Geol. 163, 41–54.
Du, W., Wang, G., 2016. A one-step newmark displacement model for probabilistic seismic slope displacement hazard analysis. Eng. Geol. 205, 12–23.
Godt, J., Şener, B., Verdin, K., Wald, D., Earle, P., Harp, E., Jibson, R., 2008. Rapid assessment of earthquake-induced landsliding. In: Proceedings of the First World Landslide Forum. United Nations University, Tokyo, pp. 392–395.
Gorum, T., Korup, O., van Westen, C.J., van der Meijde, M., Xu, C., van der Meer, F.D., 2014. Why so few? Landslides triggered by the 2002 Denali earthquake, Alaska. Quat. Sci. Rev. 95, 80–94.
Grant, A., Wartman, J., Abou-Jaoude, G., 2016. Multimodal method for coseismic landslide hazard assessment. Eng. Geol. 212, 146–160.
Guzzetti, F., Mondini, A.C., Cardinali, M., Fiorucci, F., Santangelo, M., Chang, K.T., 2012. Landslide inventory maps: new tools for an old problem. Earth Sci. Rev. 112 (1–2), 42–66.
Harp, E.L., Jibson, R.W., 1996. Landslides triggered by the 1994 Northridge, California,

earthquake. Bull. Seismol. Soc. Am. 86 (1B), S319–S332.
Harp, E.L., Wilson, R.C., 1995. Shaking intensity thresholds for rock falls and slides: evidence from 1987 Whittier narrows and superstition hills earthquake strong-motion records. Bull. Seismol. Soc. Am. 85 (6), 1739–1757.
Harp, E.L., Keefer, D.K., Sato, H.P., Yagi, H., 2011. Landslide inventories: the essential part of seismic landslide hazard analyses. Eng. Geol. 122 (1–2), 9–21.
Hartzell, S.H., Carver, D.L., King, K.W., 1994. Initial investigation of site and topographic effects at Robinwood Ridge, California. Bull. Seismol. Soc. Am. 84 (5), 1336–1349.
Hsieh, S.Y., Lee, C.T., 2011. Empirical estimation of the newmark displacement from the arias intensity and critical acceleration. Eng. Geol. 122 (1), 34–42.
Huang, R.Q., Li, W.L., 2009. Analysis of the geo-hazards triggered by the 12 May 2008 Wenchuan earthquake, China. Bull. Eng. Geol. Environ. 68 (3), 363–371.
Ishihara, K., Okusa, S., Oyagi, N., Ischuk, A., 1990. Liquefaction-induced flow slide in the collapsible loess deposit in Soviet Tajik. Soils Found. 30 (4), 73–89.
Jefferson, I.F., Evstatiev, D., Karastanev, D., Mavlyanova, N.G., Smalley, I.J., 2003. Engineering geology of loess and loess-like deposits: a commentary on the Russian literature. Eng. Geol. 68 (3–4), 333–351.
Jibson, R.W., 1993. Predicting earthquake-induced landslide displacements using Newmark's sliding block analysis. Transp. Res. Rec. 1411, 9–17.
Jibson, R.W., Harp, E.L., Michael, J.A., 2000. A method for producing digital probabilistic seismic landslide hazard maps. Eng. Geol. 58 (3–4), 271–289.
Jin, C.S., Huang, N.A., 1996. Engineering Earthquake. China Water Conservancy and Hydropower Press, Beijing (in Chinese).
Kamp, U., Growley, B.J., Khattak, G.A., Owen, L.A., 2008. GIS-based landslide susceptibility mapping for the 2005 Kashmir earthquake region. Geomorphology 101, 631–642.
Keefer, D.K., 1984. Landslides caused by earthquakes. Geol. Soc. Am. Bull. 95 (4), 406–421.
Keefer, D.K., 2002. Investigating landslides caused by earthquakes-a historical review. Surv. Geophys. 23 (6), 473–510.
Keefer, D.K., Wilson, R.C., 1989. Predicting earthquake-induced landslides, with emphasis on arid and semi-add environments. In: Landslides in a Semi-Arid Environment. vol. 2. pp. 118–149.
Lee, C.T., Huang, C.C., Lee, J.F., Pan, K.L., Lin, M.L., Dong, J.J., 2008. Statistical approach to earthquake-induced landslide susceptibility. Eng. Geol. 100 (1–2), 43–58.
Murphy, W., 2006. The role of topographic amplification on the initiation of rock slopes failures during earthquakes. In: NATO Science Series, Landslides from Massive Rock Slope Failure, Part 2. vol. 49. pp. 139–154.
Owen, L.A., Kamp, U., Khattak, G.A., Harp, E.L., Keefer, D.K., Bauer, M.A., 2008. Landslides triggered by the 8 October 2005 Kashmir earthquake. Geomorphology 94 (1–2), 1–9.
Prior, D.B., Suhayda, J.N., 1979. Application of infinite slope analysis to subaqueous sediment instability, Mississippi delta. Eng. Geol. 14 (1), 1–10.
Refice, A., Capolongo, D., 2002. Probabilistic modeling of uncertainties in earthquake-induced landslide hazard assessment. Comput. Geosci. 28 (6), 735–749.
Roberto, R., 2000. Seismically induced landslide displacements: a predictive model. Eng. Geol. 58 (3–4), 337–351.
Rodríguez, C.E., Bommer, J.J., Chandler, R.J., 1999. Earthquake-induced landslides: 1980–1997. Soil Dyn. Earthq. Eng. 18 (5), 325–346.
Saade, A., Abou-Jaoude, G., Wartman, J., 2016. Regional-scale co-seismic landslide assessment using limit equilibrium analysis. Eng. Geol. 204, 53–64.
Sato, H.P., Hasegawa, H., Fujiwara, S., Tobita, M., Koarai, M., Une, H., Iwahashi, J., 2007. Interpretation of landslide distribution triggered by the 2005 northern Pakistan earthquake using SPOT 5 imagery. Landslides 4 (2), 113–122.
Sepúlveda, S.A., Murphy, W., Jibson, R.W., Petley, D.N., 2005. Seismically induced rock slope failures resulting from topographic amplification of strong ground motions: the case of Pacoima Canyon, California. Eng. Geol. 80 (3–4), 336–348.
Shi, J.S., Wu, L.Z., Wu, S.R., Li, B., Wang, T., Xin, P., 2016. Analysis of the causes of large-scale loess landslides in Baoji, China. Geomorphology 264, 109–117.
Song, J., Gao, Y.F., Rodriguez-Marek, A., Feng, T.G., 2017. Empirical predictive relationships for rigid sliding displacement based on directionally-dependent ground motion parameters. Eng. Geol. 222, 124–139.
Sun, J.Z., Chen, X., Wang, Y.Q., 2004. Geotechnical slope collapse, three-level evaluation predict earthquake. Earthquake Res. 27 (3), 256–264 (in Chinese).
Tan, C.X., Sun, W.F., Meng, J., Zhang, C.S., Wu, S.R., Shi, J.S., Li, B., Wang, T., 2015. Research on loess-paleosol engineering geology features from the borehole cores of a typical section in Baoji area, Shaanxi province, China. Environ. Earth Sci. 74 (5), 4469–4491.
The Ministry of Construction of the People's Republic of China, 2002. National Standard of the People's Republic of China "Code for Seismic Design of Buildings" GB 50011-2001. China Architecture and Building Press, Beijing.
Wang, L.M., Yuan, Z.X., Shi, Y.C., Sun, C.S., 1999. Loess seismic hazard zoning index and method of research. J. Nat. Dis. 8 (3), 87–92 (in Chinese).
Wartman, J., Dunham, L., Tiwari, B., Pradel, D., 2013. Landslides in Eastern Honshu induced by the 2011 Tohoku earthquake. Bull. Seismol. Soc. Am. 103 (2B), 1503–1521.
Wieczorek, G.F., Wilson, R.C., Harp, E.L., 1985. Map showing slope stability during earthquakes in San Mateo County, California. In: U.S. Geological Survey Miscellaneous Investigations Series Map I 1257E.
Wilson, R.C., Keefer, D.K., 1983. Dynamic analysis of a slope failure from the 6 August 1979 Coyote Lake, California, earthquake. Bull. Seismol. Soc. Am. 73 (3), 863–877.
Wilson, R.C., Keefer, D.K., 1985. Predicting areal limits of earthquake induced landsliding. Geol. Surv. Prof. Pap. 1360, 317–345.
Wu, L.Z., Zhou, Y., Sun, P., Shi, J.S., Liu, G.G., Bai, L.Y., 2017. Laboratory characterization of rainfall-induced loess slope failure. Catena 150, 1–8.
Xu, C., Dai, F.C., Xu, X.W., Lee, Y.H., 2012. GIS-based support vector machine modeling of earthquake-triggered landslide susceptibility in the Jianjiang River watershed, China. Geomorphology 145–146, 70–80.
Xu, C., Xu, X.W., Yao, X., Dai, F.C., 2014. Three (nearly) complete inventories of landslides triggered by the May 12, 2008 Wenchuan Ww 7.9 earthquake of China and their spatial distribution statistical analysis. Landslides 11 (3), 441–461.
Zhang, Z., Wang, T., Wu, S., Tang, H., Liang, C., 2017. The role of seismic triggering in a deep-seated mudstone landslide, China: Historical reconstruction and mechanism analysis. Eng. Geol. 226 (Supplement C), 122–135.